

# InP-based Negative Feedback Avalanche Diodes

Mark A. Itzler\*, Xudong Jiang, Bruce Nyman, Krystyna Slomkowski  
Princeton Lightwave Inc., 2555 US Route 130 South, Cranbury, NJ 08512

## ABSTRACT

The operation of InP-based single photon avalanche diodes (SPADs) in Geiger mode provides great utility for the detection of single photons at near-infrared wavelengths between 1.0 and 1.6  $\mu\text{m}$ . However, SPADs have performance limitations with respect to photon counting rate and the absence of photon number resolution that, at the most fundamental level, can be traced back to the positive feedback inherent in the impact ionization-driven avalanche process. In this paper, we describe the inclusion of negative feedback with best-in-class InP-based single photon avalanche diode (SPAD) structures to form negative feedback avalanche diodes (NFADs) in which many of the present limitations of SPAD operation can be overcome. The use of thin film resistors as monolithic passive negative feedback elements ensures rapid self-quenching with very low parasitic effects and wafer-level integration for creating multi-element NFAD arrays. To our knowledge, this is the first demonstration of this approach with InP-based avalanche diode structures. We present NFAD device properties, including pulse response, quenching dynamics, and photon counting performance parameters such as photon detection efficiency.

**Keywords:** avalanche photodiodes, single photon detector, negative feedback, NFAD, InP, InGaAs, 1.5 micron

## 1. INTRODUCTION

From the perspective of performance, reliability, and cost, the most practical photodetector available today with single photon sensitivity between 1.0 and 1.6  $\mu\text{m}$  is the InGaAs/InP single photon avalanche diode (SPAD). However, for general usage—especially free-running operation—even the best InP-based SPADs have photon counting rate limitations in the range of 1 MHz, and these detectors do not have the ability to resolve the number of photons in a detected optical pulse. For high-performance photon counting applications such as long distance free-space optical communications[1], quantum cryptography[2], and long-range lidar measurements[3], single photon detectors with much faster counting rates in the range of 100 MHz to 1 GHz will be essential, and the ability to resolve photon number will provide considerable value in many cases. Additionally, SPADs require complex external electronic circuitry to control on/off gating of the device (in gated-mode operation) or avalanche quenching (in free-running operation), and for higher count rates, these electronics will become increasingly challenging.

A primary shortcoming of conventional SPADs is the positive feedback inherent in their avalanche dynamics and performance degradation associated with it. With the goal of radically improving upon these structures, we have added monolithically integrated negative feedback elements to best-in-class SPAD structures to create negative feedback avalanche diodes (NFADs) with self-limiting avalanches exhibiting highly deterministic gain values. An optimized implementation of the NFAD concept can lead to dramatically smaller avalanches (e.g.,  $\sim 10^5 - 10^6$  carriers) with extremely tight distributions [i.e.,  $F(M) \rightarrow 1$ ]. With a sufficiently small avalanche size, carrier trapping will be greatly reduced, and afterpulsing should no longer limit the repetition rate. Additionally, smaller avalanches result in reduced optical crosstalk when SPADs are fabricated in array formats because the number of photons re-emitted by hot carrier luminescence is proportional to the number of carriers flowing (generally, one photon per  $10^5$  to  $10^6$  carriers). When correctly implemented, the NFAD design is also extremely simple to operate: with just a fixed dc bias voltage corresponding to the sum of the diode avalanche breakdown voltage  $V_b$  and the desired excess bias  $V_{ex}$ , the NFAD will independently execute the entire arm, avalanche, quench, and re-arm cycle and generate an output pulse every time an avalanche event is induced. With highly deterministic gains providing much lower excess noise, it also becomes possible to sum the outputs of multiple NFADs to obtain quantized signals capable of resolving photon number.

---

\* mitzler@princetonlightwave.com, tel: (609)495-2551, fax: (609)395-9113

Our use of monolithically integrated passive negative feedback elements ensures very low parasitic effects as well as the benefits of wafer-level integration for creating multi-element matrices of NFADs. While resistive negative feedback has been introduced for silicon-based devices, to our knowledge this is the first demonstration of this approach with InP-based avalanche diode structures. In this paper, we present characterization data for basic NFAD device properties such as pulse response, quenching dynamics, and the dependence of these properties on excess bias and input photon number. We also present data for photon detection efficiency (PDE) extracted from measurements of the detection probability as a function of input photon number.

### 1.1 Limitations of SPAD Performance

SPADs are avalanche diode structures designed to operate above their breakdown voltage  $V_b$ , so that a single photoexcited carrier can induce a macroscopic current by avalanche breakdown. Many of the shortcomings of conventional SPAD performance are related to the positive feedback inherent in the impact ionization process above  $V_b$ : if electrons and holes both have finite impact ionization coefficients, then every carrier created by impact ionization tends to create additional carriers, leading to a runaway avalanche. This positive feedback can be very useful when the device is operated as a digital switch: the avalanche current can rapidly grow to be detectable using a comparator on the SPAD output with an appropriate threshold setting. Once an avalanche is detected, it is quenched by forcing the bias below  $V_b$ .

However, the stochastic nature of the positive feedback impact ionization process leads to enormous fluctuations in the number of carriers created per unit time. For linear mode operation with a multiplication gain  $M$ , this can be described by the excess noise factor  $F(M) \equiv \langle M^2 \rangle / \langle M \rangle^2$ .  $F(M)$  contributes to the shot noise through a term proportional to  $I_p M^2 F(M)$ , where  $I_p$  is the primary photocurrent (i.e., prior to multiplication). Although  $F(M)$  depends on the material properties, for sufficiently large gains (e.g.,  $M > 10^4$ ), all avalanche diodes with a non-zero impact ionization coefficient ratio  $k$  will exhibit fluctuations in avalanche magnitude that make photon number resolution impossible. Although it is not correct to refer to SPADs as having a well-defined gain (because their operation is defined by a self-sustaining avalanche prior to quenching), they are still subject to the same fluctuations in the number of carriers created per unit time that give rise to excess noise. Therefore, dramatic variations in carrier flow per SPAD avalanche event tend to inhibit any accurate determination of how many photons triggered the avalanche.

Repetition rate limitations are a major challenge for SPADs and, to date, have been dominated by a phenomenon called “afterpulsing.” Given the limits on the speed of external quenching, typical SPAD avalanches involve the flow of a large number of carriers ( $\sim 10^7 - 10^8$ ), and some fraction of these carriers tend to be trapped at defect sites in the avalanche region. Trapped carriers are then released with some characteristic de-trap time governed by the nature of the traps, the temperature, and the applied electric field. If the SPAD is re-armed before substantially all of the trapped carriers are released, then de-trapped carriers are likely to initiate a dark count, in this case referred to as an afterpulse. All InGaAs/InP SPADs that are armed for durations of  $\sim 1$  ns or longer tend to exhibit significant afterpulsing if re-arming occurs in much less than  $1 \mu\text{s}$  following an avalanche detection, limiting useful detection rates to  $\sim 1$  MHz. It is known that the severity of afterpulsing is related to how many carriers flow through the multiplication region during previous avalanches [4]. Very short arming durations of well under 1 ns have been shown to reduce afterpulsing effects [5,6], presumably by limiting the charge flow per avalanche, but this mode of operation can be highly constraining for many applications.

### 1.2 Benefits of NFAD Performance

To surmount the present obstacles to higher counting repetition rate and photon number resolution using SPADs, we have introduced negative feedback to the conventional SPAD avalanche process to beneficially modify the device avalanche dynamics. The goal of this approach is to achieve extremely consistent passive quenching by the monolithic integration of a suitable negative feedback element, e.g., a suitable thin film resistor in series with the SPAD structure. As we will describe, an appropriate implementation of this concept can lead to rather small avalanches (e.g.,  $\sim 10^5 - 10^6$  carriers), in which case carrier trapping will be greatly reduced and afterpulsing will no longer limit the photon counting rate relative to other bandwidth-limiting factors. If an array of these detectors is fabricated with all anodes connected and all cathodes connected, then the single output signal from the array will exhibit quantized current pulses

whose amplitudes indicate the number of detectors that have avalanched. Even if one cell of this array experiences some “dead time” following a detection event, remaining cells will still be armed. In this way, multiplexed structures can support even higher repetition rates.

The introduction of negative feedback using a load resistor is conceptually equivalent to passive quenching, but historically, passive quenching has been introduced through hybrid integration approaches that invariably introduce large parasitic effects. With an ideal monolithic integration, the amount of charge flow  $Q$  required prior to avalanche quenching is simply the product of the avalanche diode depletion capacitance  $C_d$  and the excess bias  $V_{ex}$ , i.e.,  $Q = C_d \times V_{ex}$ . With optimal implementation, each avalanche involves this same amount of charge flow  $Q$ , and  $Q$  can be made quite small through appropriate scaling of  $C_d$ . (The magnitude of the excess bias  $V_{ex}$  will be dictated by operational targets for PDE since PDE increases with larger  $V_{ex}$ .)

The use of negative feedback with avalanche diodes has received some attention in the literature on detectors for nuclear physics experiments [7–12], but these treatments have focused exclusively on Si detectors. These Si-based structures have been referred to by a variety of labels, most frequently as “metal-resistance-semiconductor” (MRS) APD structures. The only previously reported approach to using a monolithic negative feedback structure that achieves self-quenching in an InP-based avalanche diode structure is the use of an epitaxial heterobarrier grown right above the avalanche diode that promotes avalanche charge pile-up to reduce the internal electric field, thereby quenching the avalanche. [13] To distinguish our new detectors from conventional InGaAs/InP SPADs, as well as from conventional hybrid approaches to passive quenching, we have referred to them as “negative feedback avalanche diodes,” or NFADs.

## 2. NFAD DEVICE DESIGN AND CHARACTERIZATION TEST SET

Although the NFAD promises significant improvements with respect to counting rate and photon number resolution relative to SPAD performance, certain fundamental attributes—such as the trade-off between dark count rate (DCR) and photon detection efficiency (PDE)—will still be dictated by the underlying avalanche diode structure. [14,15] To provide reference data for the underlying SPAD structure upon which the NFAD is based, we fabricated 1550 nm SPAD reference devices without negative feedback elements with device diameters that matched those of the NFAD devices. Using a measurement technique employing short pulse (1 ns) gating [16], we have measured DCR and PDE for a 25  $\mu\text{m}$  active area reference SPAD at operating temperatures of 243 K and 223 K; see Figure 1. The DCR of <200 Hz obtained for PDE values of ~15% at 223 K is lower than any 1550 nm SPAD results we have seen reported for comparable conditions, and this performance has been confirmed with measurements by other researchers [17] on other devices from the same process lot. This improved performance relative to earlier generations of PLI 1550 nm SPADs is related to structural changes that included lowered the electric field in the multiplication region for more effective suppression of dark carrier generation by trap-assisted tunneling.

The fabrication of NFADs based on our underlying SPAD avalanche diode structure was carried out using thin film NiCr resistor meander lines integrated on the surface of the diode structure. We fabricated devices with a variety of active area sizes and feedback resistance values. In this paper, we will present results from two device types: D3F7 had a 58  $\mu\text{m}$  optical active area diameter with an integrated resistance of ~90 k $\Omega$ ; and D1F5 had a 34  $\mu\text{m}$  optical diameter with a resistance of ~40 k $\Omega$ . Devices were assembled into either a TO-style package or a 14-pin butterfly-style package with direct fiber coupling to the device. Data reported below were obtained for an operating temperature of 230 K.

The test set-up for characterizing the NFAD devices differs substantially from that used for SPAD characterization. To a significant degree, NFAD operation is far simpler because it is biased with a fixed dc voltage, in contrast to the somewhat complicated gating circuitry required for SPAD operation. Figure 2 contains a schematic illustration of the test set used for initial NFAD measurements. The dc bias voltage is provided by a Keithley 236 Source Measure Unit using a Picosecond Pulse Labs bias tee. The NFAD device under test is capacitively coupled via the bias tee to a Minicircuits amplifier that provides 24 dB of electrical gain. The amplifier output is fed directly to a Tektronix digital sampling oscilloscope, and data was captured frame by frame from the oscilloscope.

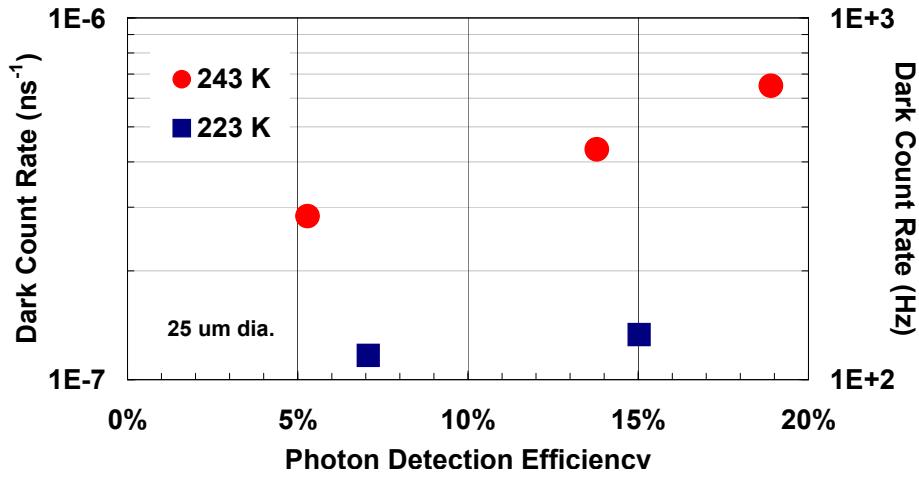


**Figure 1.** Dark count rate (DCR) versus photon detection efficiency (PDE) for 1550 nm reference SPADs with 25  $\mu\text{m}$  diameter at 223 K and 243 K.

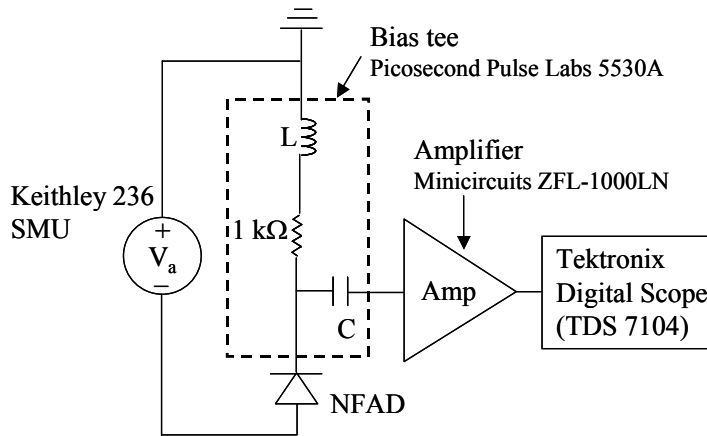


**Figure 2.** Schematic of test set-up used for characterizing NFAD devices.

#### 4. NFAD DATA FOR DARK COUNT BEHAVIOR

Preliminary data obtained for the NFAD pulse response to dark counts provides considerable insight into the behavior of these devices. Device behavior is somewhat stochastic, and so it is necessary to collect a reasonable amount of pulse shape data to confirm “typical” NFAD pulse behavior. Moreover, this behavior is strongly dependent on the magnitude of the excess bias voltage, so characterization over a range of excess bias voltages is highly informative.

##### 4.1 NFAD pulse response to dark carriers

In Figure 3, we present an illustrative example of an NFAD pulse response to a dark carrier. The device is of the design D3F7, with an active area diameter of 58  $\mu\text{m}$  and a feedback resistance of  $\sim 90\text{ k}\Omega$ . Data were obtained at an operating temperature of 230 K and an applied dc bias of 71.5 V, corresponding to an excess bias of about 0.5 V. The voltage noise in the absence of device current flow is about 5 mV p-p. A negative-going peak of about 15 to 20 mV is measured in response to a dark count occurring in the NFAD. The overall pulse width corresponding to the total time

for avalanching and quenching is about 15 to 20 ns. The rise time to reach the peak current flow is quite short—on the order of 2 to 3 ns—with the pulse width being dominated by the dissipation of this current flow through the quenching process induced by the negative feedback. The decay of the output voltage to 0 V occurs when avalanche quenching terminates current flow.

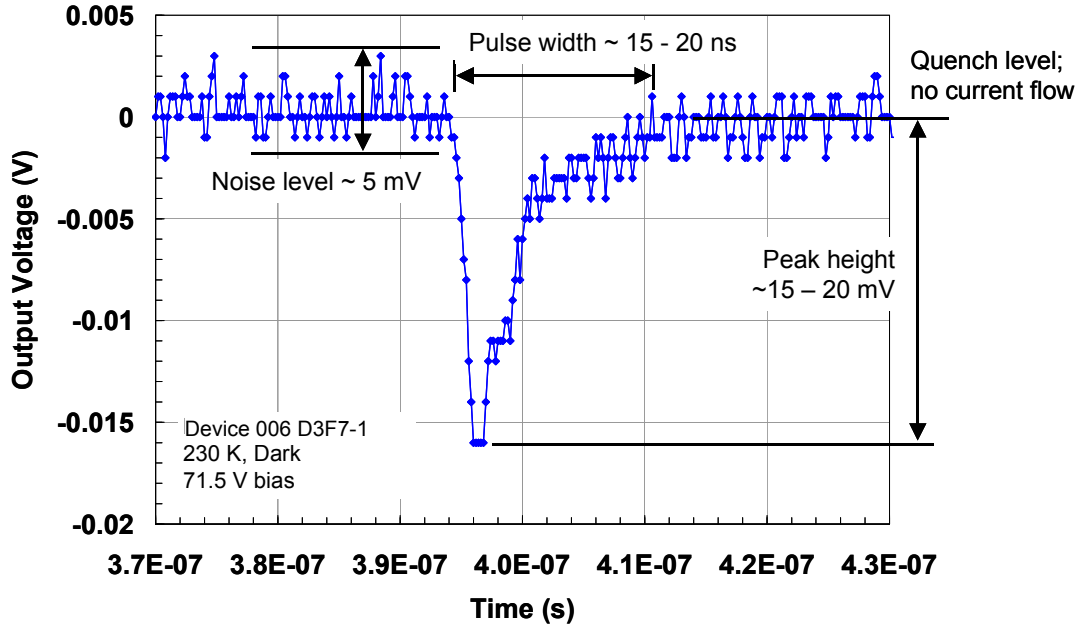


**Figure 3.** Illustrative example of an NFAD pulse response to a dark count for device type D3F7 consisting of a 58  $\mu\text{m}$  active area diameter and a feedback resistance of  $\sim 90\text{ k}\Omega$ . The excess bias was nominally 0.5 V.

#### 4.2 NFAD pulse response vs. excess bias and persistent current phenomena

A critical aspect of the avalanche quenching process in an NFAD—or in any passive quenching scheme—is that the instantaneous current flow must be reduced below a threshold “quenching” current  $I_q$  below which rapid spontaneous quenching is probable. [18,19] The occurrence of spontaneous quenching is intimately related to how many carriers are present in the junction at a given time  $T_0$ . The probability of quenching by some later time  $T > T_0$  is given by the joint probability that the sequence of multiplication events for *every* individual carrier in the avalanche region at  $T_0$  dies out by time  $T$ . [20] For current flow on the order of  $I_q$ , a persistent current may flow for an appreciable period of time before spontaneous quenching occurs.

The pulse behavior in Figure 4(a) demonstrates how a persistent current can flow, with a corresponding fixed level of the signal voltage  $V_{\text{sig}}$ , before the NFAD spontaneously quenches, bringing the measured signal back to zero. In the figure, this persistent current is indicated by the  $\sim 10\text{ ns}$  plateau that interrupts the falling edge of the pulse shape. The equivalent circuit [18] in Figure 4(b) includes a switch  $S$  that is closed when the diode is generating avalanche current, and the continued flow of persistent current corresponds to this switch remaining closed. The spontaneous quenching of avalanche current corresponds to the opening of this switch, after which the NFAD is re-armed by re-charging the diode capacitance  $C_d$ .

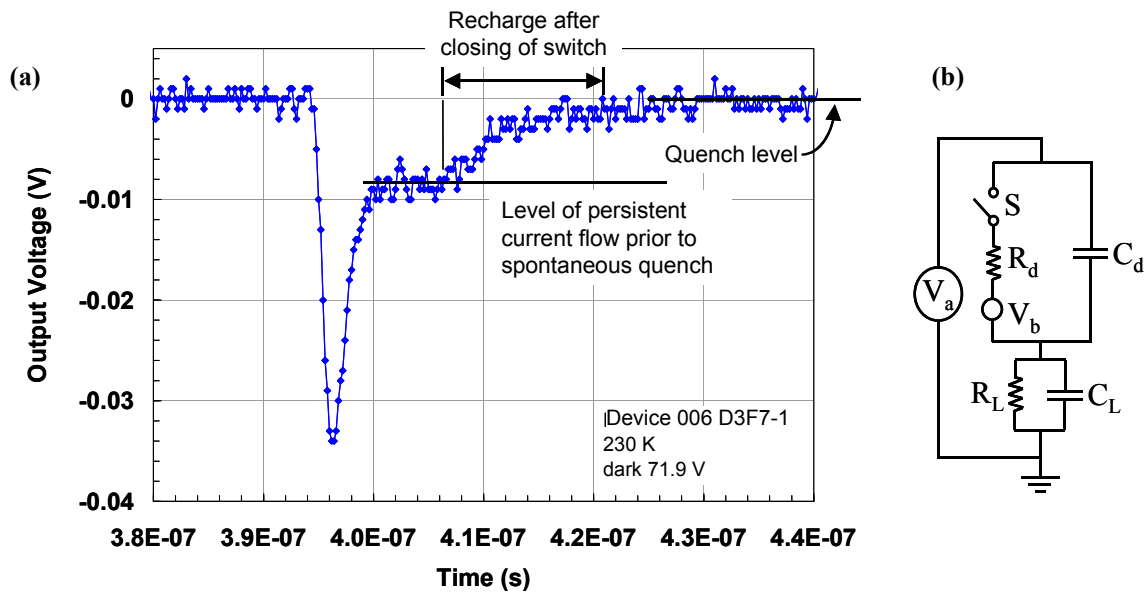


**Figure 4.** (a) NFAD pulse response to a dark count for device type D3F7 at  $\sim 0.9$  V excess bias exhibiting persistent current for about 10 ns before the device spontaneously quenched. (b) The equivalent circuit used to model NFAD performance includes a switch S that is closed whenever avalanche current is flowing. The opening of S corresponds to the spontaneous quenching process.

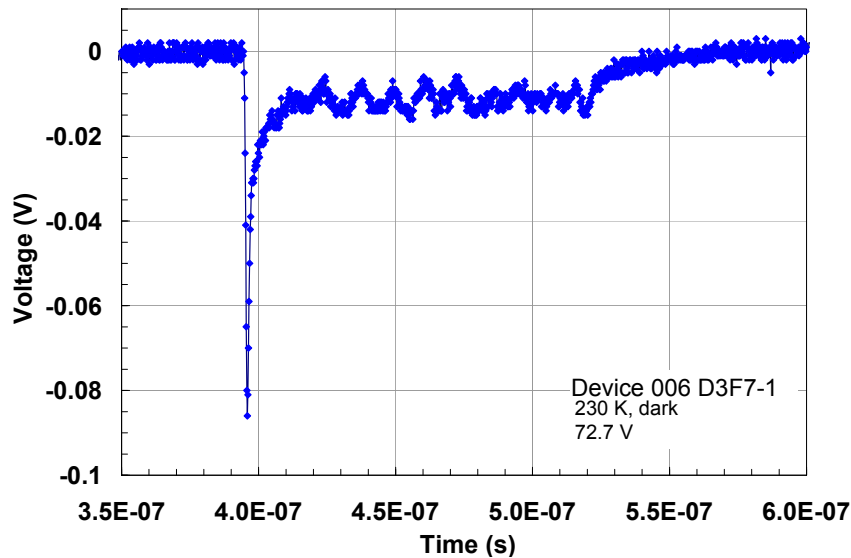


**Figure 5.** NFAD behavior for a larger excess bias of  $\sim 1.7$  V for device type D3F7. This particular pulse response shows a rather long period ( $\sim 120$  ns) of persistent current flow before spontaneous quenching occurs. The periodic structure found during persistent current flow is categorically different from the noise observed in the absence of current flow (near  $V_{sig} = 0$ ).

As the excess bias voltage is increased, we observe an increase in the average duration of the persistent current. In Figure 5, we illustrate a dark count pulse response for the same D3F7 device taken at a larger excess bias of  $\sim 1.7$  V. Following the initial large amplitude peak in the pulse response, there is persistent current flow for  $\sim 120$  ns at a voltage level on the order of 15 to 20 mV, after which the current flow spontaneously quenches. There is also a quite

pronounced oscillatory behavior of the response signal during this period of persistent current flow, with a strong component having a  $\sim 10$  ns periodicity. We have seen this phenomenon consistently for every NFAD we have tested, and we believe that these oscillations may be fundamentally related to the carrier dynamics involved with the marginal avalanche that occurs in maintaining the persistent current. We will be doing more in-depth modeling of these carrier dynamics in the future with the goal of explaining this oscillatory persistent current behavior.

We have confirmed experimentally that the gradual increase in the duration of the persistent current for larger excess bias voltages continues up to a critical range of excess bias at which the persistent current duration effectively diverges. In Figure 6, we present data measured for the same device of type D3F7 at a bias voltage of 73.5 V, corresponding to an overbias of  $\sim 2.5$  V. At this overbias, the device does not readily quench and spends most of its time carrying persistent current. Because the NFAD is ac-coupled to the amplifier that follows it (see Figure 2), when the persistent current dominates the signal response, this signal corresponds to  $V_{sig} = 0$ , and the quench level actually corresponds to a positive voltage level. Figure 6 shows a rare event in which the device spontaneously quenches, corresponding to a rise in  $V_{sig}$  to between +15 and +20 mV. However, within  $\sim 100$  ns, the NFAD avalanches again, leading to a total swing in  $V_{sig}$  of nearly 90 mV, followed by a fast recovery back to the persistent current level at  $V_{sig} = 0$ . In this mode of operation, there is so much persistent current flowing through the device prior to a quenching event, it is likely that afterpulsing induces rather immediate subsequent avalanches once the device has re-armed. In fact, we have seen evidence of avalanching that occurs before the NFAD has fully re-charged. Since this situation corresponds to a lower value for the instantaneous excess bias, one would expect to see a lower amplitude avalanche peak, and this is exactly what we have seen.

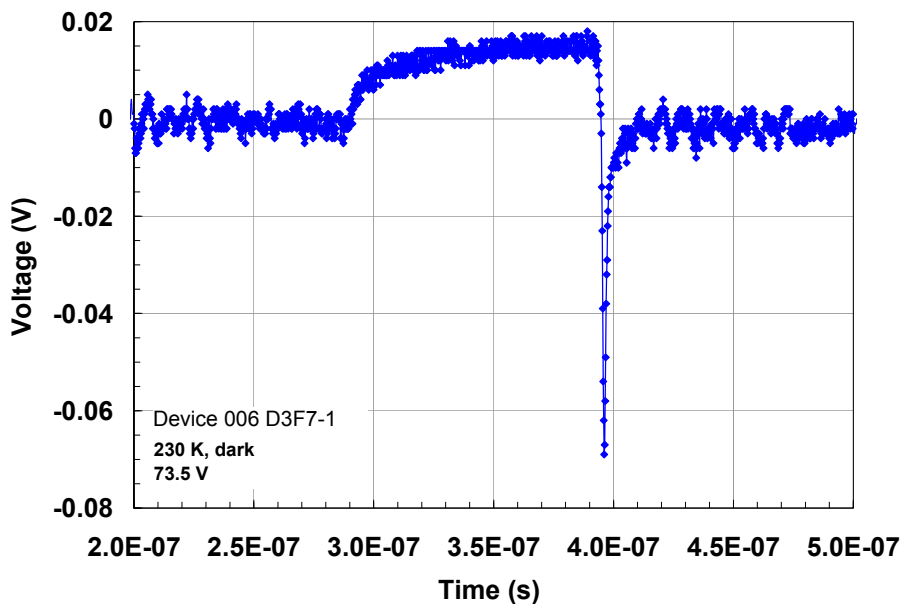


**Figure 6.** NFAD behavior for larger overbias of  $\sim 2.5$  V for device type D3F7. Because the NFAD output is ac coupled, the  $V_{sig} = 0$  level corresponds to a persistent current that is flowing nearly continuously. This graph captures a rare event in which the current quenches, re-arms, and quickly avalanches again within  $\sim 100$  ns.

Although there is no practical utility to operating the NFAD when persistent currents dominate, there is value in studying the device in this limit to confirm certain fundamental aspects of the device behavior. With our present understanding of the persistent current, one concludes that it is not possible for the NFAD to exhibit a detection event (i.e., a peak response) while the persistent current is flowing. In this state, the internal voltage across the diode is essentially equivalent to the breakdown voltage, and there is no excess charge residing on the diode capacitance to give rise to a detectable current pulse. Experimentally, we find this to be the case. A sharp avalanche peak occurs only after the NFAD has quenched and re-armed, as in Figure 6, and never occurs from the persistent current signal level.

Data obtained at excess bias voltages in which persistent current dominates also confirm additional expected trends in the NFAD behavior. The level of the persistent current above the zero-current quenched state is expected to rise linearly with the excess bias, and we find this trend in the data, as illustrated in Figure 7. A simple model for estimating the persistent current  $I_p$  can be arrived at by noting that  $I_p \sim V_{ex}(R_L + R_d) \approx V_{ex}R_L$ , where  $V_{ex}$  is the excess bias, and the load resistance  $R_L$  is much greater than the effective dynamic resistance  $R_d$  of the photodiode (in this case, a few  $k\Omega$ ). Assuming that  $I_p$  is dropped across a  $50\ \Omega$  load and taking an amplifier gain of 10, one obtains the dashed line fit to the pulse persistent current level shown in Figure 7. (The measured amplifier gain of 15.8 leaves us with a minor discrepancy that will require a more detailed analysis to explain.)

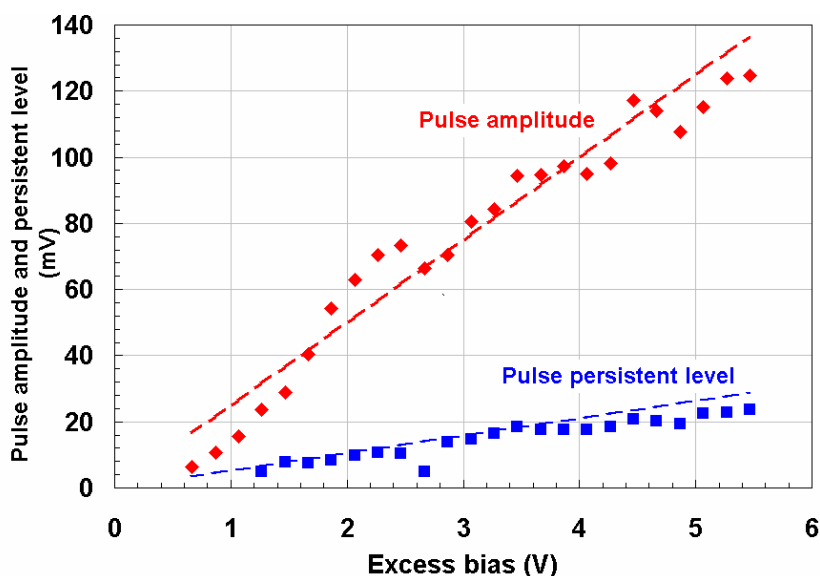


**Figure 7.** Dependence of NFAD dark pulse amplitude and persistent level on excess bias. These data were obtained from a series a pulse captures for increasingly larger excess biases (in 0.2 V steps) such as those presented in Figures 3 – 6. Dashed lines are simple model fits described in the text.

The overall voltage excursion of the pulse response—i.e., the pulse peak amplitude—is also expected to scale linearly with the excess bias. When judged by the total swing between  $V_{sig}$  at the quenched level and  $V_{sig}$  at the maximum voltage excursion of the pulse (e.g., +15 mV and –70 mV, respectively, in Figure 6), we find this behavior to be true as well. In Figure 7, we present pulse amplitude data obtained over a range of excess bias voltages that exhibits the anticipated linear dependence. To make a very rough estimate, one might assume that the pulse amplitude is dictated by  $V_{ex}/R_d$ . The dashed fit to the pulse amplitude data shown in the figure is found if we assume that  $R_d \sim 20\ k\Omega$ . This  $58\ \mu m$  active diameter NFAD is expected to have  $R_d$  closer to  $\sim 5\ k\Omega$  (this can be confirmed using reference SPAD devices), but this estimate to within a factor of 4 indicates that the  $V_{ex}/R_d$  approximation gives the correct order of magnitude for the pulse amplitude slope.

### 4.3 Dependence of total NFAD pulse width (total quench time) on excess bias

The occurrence of persistent current in the NFAD pulse response lengthens the time it takes for the device to quench and broadens the effective pulse width. It also results in greater charge flow per avalanche, which is bound to exacerbate afterpulsing effects. Therefore, one of our NFAD design goals is to effectively eliminate the persistent current. To obtain an initial assessment of the dependence of the quench time on overbias, we have extracted overall pulse width for the series of pulses with excess bias increasing by 0.2 V increments and plotted it as a function of excess bias. For the sake of this discussion, the “quench time” is equated with the “overall pulse width”, as determined

by the total time elapsed between the initial increase of the signal above the noise level at  $V_{\text{sig}} = 0$  and the return of the signal to  $V_{\text{sig}} = 0$  following the quench process.

To estimate the total quench time for a given overbias, we have used “typical” pulses obtained for each bias voltage and, despite some scatter in the measured data, the trend in quench time versus bias voltage can be clearly seen in Figure 8(a). These data were obtained for both the D3F7 design (58  $\mu\text{m}$  active area and  $\sim 90\text{ k}\Omega$  resistance) and D1F5 design (34  $\mu\text{m}$  active area and  $\sim 40\text{ k}\Omega$  resistance). As shown in Figure 3, in the absence of persistent current, the total pulse width is dominated by the intrinsic quench time and, though dependent on excess bias, is on the order of 20 ns. For larger total quench times, these values are dominated by the persistent current.

The data in Figure 8 are fit reasonably well by an exponential increase in total quench time with increasing bias. Since we do not yet have a model based on physical principles, this fit is still phenomenological. However, if the persistent current  $I_p$  is sufficiently close to quench current  $I_q$ , one may assume that quenching will occur. It is also reasonable to assume that the quench time  $T_q$  would have a strong dependence on  $(I_p - I_q)$ . If we assume that  $T_q \sim \exp[(I_p - I_q)/I_q]$ , then since  $I_p \sim V_{\text{ex}}(R_L + R_d)$ , we expect  $T_q$  to have an exponential dependence on the excess bias, as found in Figure 8(b). Moreover, with the assumption of this functional form for  $T_q$ , it is straightforward to extract a value for  $I_q$  from our data. We obtain values for  $I_q$  of approximately 6  $\mu\text{A}$  for D3F7 and 10  $\mu\text{A}$  for D1F5. Interestingly, these values are about a factor of 10 smaller than values cited for  $I_q$  in the context of passive quenching in Si SPADs. [19]

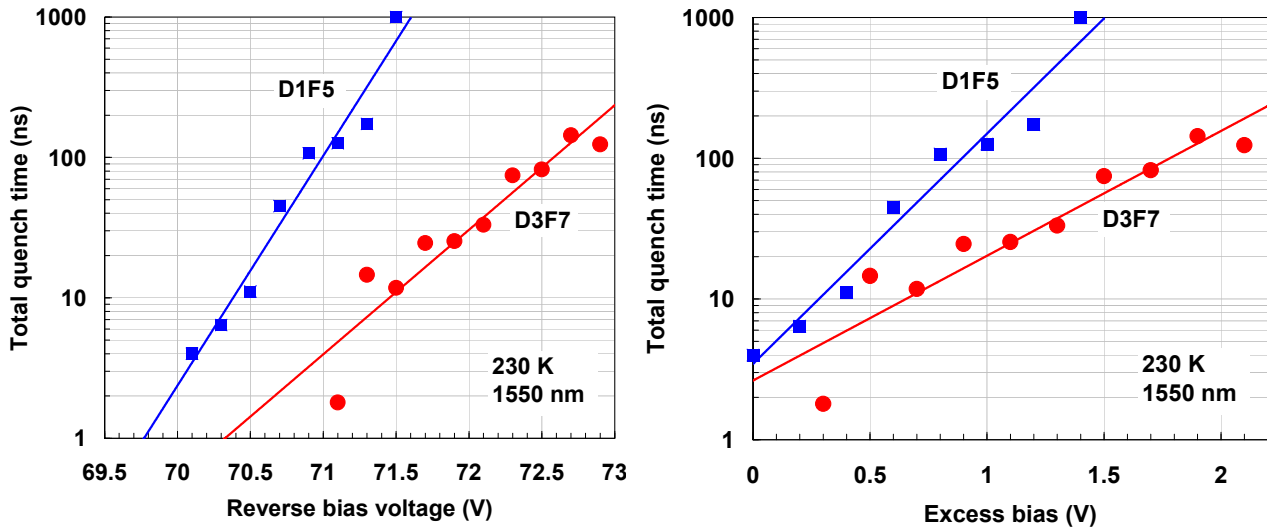


**Figure 8.** Dependence of total quench time on (a) reverse bias voltage and (b) excess bias for devices of design D1F5 and D3F7 in a 1550 nm NFAD structure. The exponential fits are phenomenological at present. D1F5, with a  $\sim 40\text{ k}\Omega$  feedback resistance, has a more rapid increase in quench time with excess bias than D3F7, which has a  $\sim 90\text{ k}\Omega$  feedback resistance.

With respect to Figure 8(b), it is also interesting to confirm that for any value of  $T_q$ , the excess bias corresponding to this  $T_q$  scales roughly inversely proportionally with the feedback resistance of the NFAD. [From the information above,  $\ln(T_q) \sim V_{\text{ex}}/(R_L I_q)$ .] Therefore, we can operate at higher  $V_{\text{ex}}$ , with consequently higher PDE, while maintaining the same  $T_q$  if we increase  $R_L$  in proportional to the increase in  $V_{\text{ex}}$ .

#### 4. NFAD RESPONSE TO OPTICAL PULSES

We characterized the response of the NFADs to optical pulses by providing short (~500 ps) 1550 nm pulses at a fixed repetition rate. To avoid long persistent currents, illuminated characterization was conducted for fairly low excess bias voltages of less than 1 V. Since we were monitoring pulse events occurring within 5 to 10 ns of the optical pulse arrival at the detector, the possibility for misidentification of dark counts for photon pulse counts was low.

In Figure 9, we exhibit the response of the NFAD to optical pulses with a large range of number of photons per pulse. Responses were obtained for about a dozen different values, but we have restricted the figure to five different values for the sake of clarity. With a very large number of photons (e.g., 10,000 or 1000), the response of the detector is very fast and very consistent since any one of the large number of photons in the pulse can initiate the NFAD avalanche response. For smaller numbers of photons per pulse, the precise time of the avalanche onset was somewhat more stochastic, but on average, a larger photon number gave a more immediate response, as expected. For 100 photons or more, there also appears to be a somewhat larger NFAD peak response for larger photon number; for example, the peak height for 1 photon per pulse was about 40 mV, while the peak height for 10,000 photons per pulse was about 75 mV. However, the consistency in peak height—to within a factor of 2—for an increase in photon number of four orders of magnitude indicates that a single negative feedback device provides rather uniform pulse responses even when the optical stimulus is dramatically different. This uniformity of response is what allows for the multiplexing of many NFADs in parallel to achieve photon number resolution.

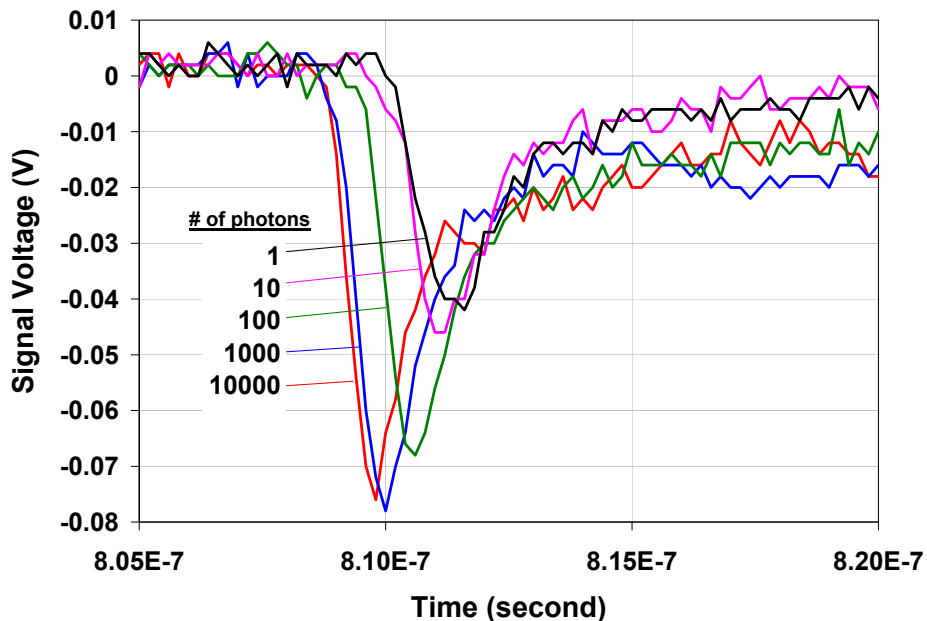


**Figure 9.** Response of the NFAD to short (~500 ps) optical pulses. Responses are shown for the number of photons per pulse ranging from 1 to 10,000 photons with an excess bias of 0.7 V and 230 K.

To accurately determine the photon detection efficiency (PDE) of a SPAD, one often relies on the use of a very small photon number per pulse (e.g., 0.1) to guarantee that the incidence of more than one photon per pulse is sufficiently low (e.g., < 1%) to avoid distorting the PDE values obtained. We have used a different approach for determining the intrinsic PDE that makes use of our measurements using a wide variation in photon number per pulse. If the probability of detecting a single photon is  $p_s$ , then the probability of not detecting a photon when it is present is  $(1 - p_s)$ . If an incident pulse has  $N$  photons, then the probability of not detecting any of these photons is  $(1 - p_s)^N$ . Therefore, the probability of a detection event  $P_{\text{det}}$  (in response to 1 or more photons) is  $P_{\text{det}} = 1 - (1 - p_s)^N$ . We have plotted this functional form for  $P_{\text{det}}$  as a function of photon number per pulse in Figure 10 for intrinsic PDE values (i.e.,

$p_s$  in the formalism just described) ranging from 2% to 7% in increments of 1%. We then assessed the probability of a detection event  $P_{det}$  using the data obtained for different photon numbers per pulse. These measured values are exhibited as solid points for two values of the excess bias. In the figure, the simulated detection probability provides an excellent fit to the measured values and allows us to extract an accurate value for the intrinsic detector PDE.

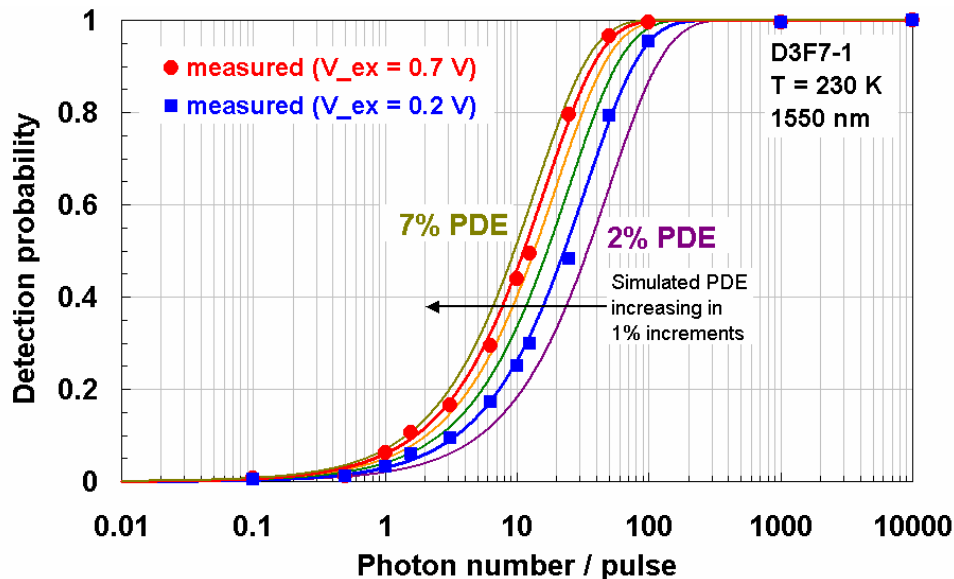


**Figure 10.** Dependence of the overall detection probability on the number of photons per pulse. Simulated detection probability vs. photon number per pulse is shown for six different values of intrinsic detector photon detection efficiency (PDE) ranging from 2% to 7% in increments of 1%. Experimental data are shown for two excess bias values, 0.2 V and 0.7 V, and are consistent with PDE values of 3% and 6 %, respectively.

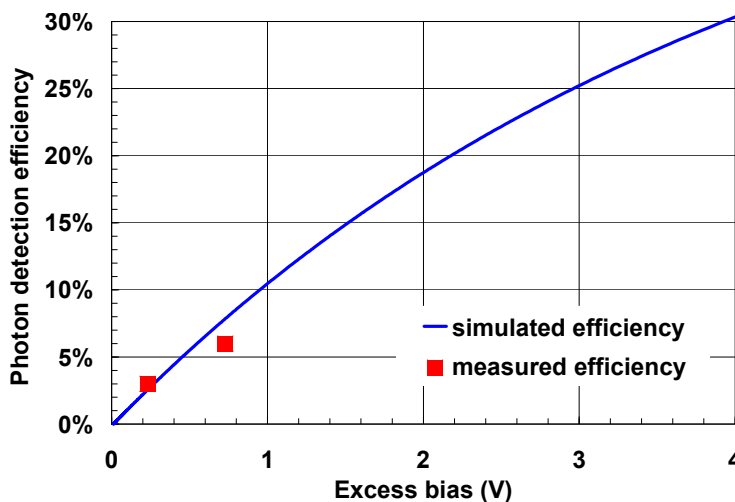


**Figure 11.** Simulation of photon detection efficiency (PDE) vs. excess bias for the NFAD used to obtain the data in Figure 10. The two PDE values extracted from the measurements presented in that figure are reasonably consistent with the simulation.

The PDE values extracted from the data in Figure 10 are compared in Figure 11 to our simulation for PDE as a function of excess bias. Although the value of 6% PDE obtained at 0.7 V excess bias is somewhat lower than the

simulated value of 7.5%, the agreement is reasonable. Larger feedback resistances will enable operation at higher PDE since the greater suppression of persistent current effects will allow for the use of larger excess biases. (Recall that long persistent currents also reduce the effective PDE since avalanches cannot be initiated from the persistent current state.) The superior performance of devices with larger feedback resistance, at least from the perspective of having shorter quench times, has already been demonstrated in Figure 8.

## ACKNOWLEDGMENTS

We are grateful to Bill Farr and Michael Krainak for valuable discussions concerning the negative feedback avalanche diode concept and its characterization. We acknowledge partial support for this work from JPL and NASA/GSFC.

## REFERENCES

- [1] Special Issue on “Free-space laser communications”, IEEE LEOS Newsletter, vol. 19 No. 5 (2005).
- [2] N. Gisin, G. Ribordy, W. Tittel, and H. Zbinden, *Rev. Mod. Phys.*, vol. 74, p. 145 – 195 (2002).
- [3] R. M. Measures, *Laser Remote Sensing - Fundamentals and Applications*, John Wiley & Sons (1984).
- [4] S. Cova, A. Lacaita, and G. Ripamonti, *IEEE Elec. Dev. Lett.* **12**, p. 685 – 687 (1991).
- [5] N. Namekata, S. Sasamori, and S. Inoue, *Opt. Express*, **14**, 10043 (2006).
- [6] Z.L. Yuan, B.E. Kardynal, A.W. Sharpe, and A.J. Shields, *Appl. Phys. Lett.* **91**, 041114 (2007).
- [7] D. Bisello, et al., *Nuclear Instruments and Methods in Physics Research A* **360**, p. 83 – 86 (1995); *ibid.* **367**, p. 212 – 214 (1995).
- [8] S. Afanasiev, et al., *Nuclear Physics B* **44**, p. 402 – 405 (1995).
- [9] D. Shushakov and V. Shubin, *Proc. SPIE* **2397**, p. 544 – 554 (1995); V. Shubin and D. Shushakov, *Proc. SPIE* **2415**, p. 94 – 103 (1995).
- [10] D. Shushakov and V. Shubin, *Proc. SPIE* **2699**, p. 173 – 183 (1996).
- [11] G. Bondarenko, et al., *Nucl. Phys. B* **61B**, p. 347 – 352 (1998).
- [12] P. Buzhan, et al., *ICFA Instrumentation Bulletin* (Fall 2001) [<http://www.slac.stanford.edu/pubs/icfa/fall01.html>]
- [13] K. Zhao, A. Zhang, Y.-h. Lo, and W. Farr, *Appl. Phys. Lett.* **91**, 081107 (2007); K. Zhao, S. You, J. Cheng, and Y.-h. Lo, *Appl. Phys. Lett.* **93**, 153504 (2008).
- [14] M.A. Itzler, R. Ben-Michael, C.-F. Hsu, K. Slomkowski, A. Tosi, S. Cova, F. Zappa, R. Ispasoiu, *J. Modern Optics* **54**, no. 2-3, p. 283 – 304 (2007).
- [15] X. Jiang, M. A. Itzler, R. Ben-Michael, and K. Slomkowski, *IEEE J. of Sel. Topics in Quantum Electronics* **13**, p. 895 – 905 (2007).
- [16] D.S. Bethune, W.P. Risk, and G.W. Pabst, *J. Modern Optics* **51**, no. 9-10, p. 1359 – 1368 (2004).
- [17] A. Tosi, A. Dalla Mora, F. Zappa, S. Cova, M. A. Itzler, and X. Jiang, *Proc. SPIE* **2777-53**, in this proceedings.
- [18] R. H. Haitz, *J. Appl. Phys.* **35**, p. 1370 – 1376 (1964).
- [19] S. Cova, M. Ghioni, A. Lacaita, C. Samori, and F. Zappa, *Appl. Opt.* **35**, p. 1956 – 1976 (1996).
- [20] M. M. Hayat, G. J. Rees, D. A. Ramirez, and M. A. Itzler, 2008 IEEE LEOS Annual Meeting Conference Proceedings, p. 230 – 231 (2008).